

## Reusable and Recyclable Graphene Masks with Outstanding Superhydrophobic and Photothermal Performances

Hong Zhong<sup>1</sup>, Zhaoran Zhu<sup>1</sup>, Jing Lin<sup>1</sup>, Chi Fai Cheung<sup>1</sup>, Vivien L. Lu<sup>2</sup>, Feng Yan<sup>3</sup>, Ching-Yuen Chan<sup>1</sup>, Guijun Li<sup>1\*</sup>

<sup>1</sup>State Key Laboratory of Ultra-Precision Machining Technology, Department of Industrial and Systems Engineering, The Hong Kong Polytechnic University, Kowloon, Hong Kong, 999077, China

<sup>2</sup>Department of Building Services Engineering, The Hong Kong Polytechnic University, Kowloon, Hong Kong, 999077, China

<sup>3</sup>Department of Applied Physics, The Hong Kong Polytechnic University, Kowloon, Hong Kong, 999077, China

Email: [mitch.li@polyu.edu.hk](mailto:mitch.li@polyu.edu.hk)

### ABSTRACT:

The 2019 coronavirus outbreak (COVID-19) is affecting over 210 countries and territories, and it is spreading mainly by respiratory droplets. The use of disposable surgical masks is common for patients, doctors and even the general public in highly risky areas. However, the current surgical masks cannot self-sterilize in order to re-use or be recycled for other applications. The resulted high economic and environmental costs are further damaging societies worldwide. Herein, we reported a unique method for functionalizing commercially available surgical masks with outstanding self-cleaning and photothermal properties. A dual-mode laser induced forward transfer method was developed for depositing few-layer graphene onto the low-melting temperature non-woven masks. Superhydrophobic states were observed on the treated masks surfaces, which can cause the incoming aqueous droplets to

bounce off. Under sunlight illumination, the surface temperature of the functional mask can quickly increase over 80 °C, making the masks reusable after sunlight sterilization. In addition, this graphene-coated mask can be recycled directly for use in solar-driven desalination with outstanding salt-rejection performance for long-term use. These roll-to-roll production-line-compatible masks can provide us with better protections against this severe virus. The environment can also benefit from the directly recycling of these masks which can be used for desalinating seawater.

**KEYWORDS:** COVID-19, superhydrophobic, photothermal, graphene, laser precision manufacturing

The recent COVID-19 outbreak had endangered over 210 countries and territories by middle April 2020, especially for those areas with high population densities.<sup>1</sup> Disposable surgical masks can prevent respiration droplets to enter the lungs, which can help to reduce the risk of getting infected, alongside with the proper hygiene hand cleaning method.<sup>2-7</sup> However, there are some limitations for the existing masks. First, although the surfaces of the surgical masks are hydrophobic, water droplets containing the dangerous viruses can remain on them.<sup>8,9</sup> Secondly, the mask has a low melting point, usually lower than 130 °C,<sup>10</sup> so it is challenging to reuse them even with the steam sterilization method. Thirdly, the used masks are challenging to recycle, because the captured viruses might stay on their surfaces. Considering the daily worldwide production rates of surgical masks are at 40 million pieces, the resulted wastes are over 15,000 tons every day. In order to process these used masks, most countries can only use incineration to treat such medical wastes. The resulting toxic gases and high carbon emission greatly harms the environment.<sup>11</sup>

Surfaces in a superhydrophobic state possess self-cleaning features which can significantly benefit the medical application.<sup>12</sup> Hydrophobic surfaces with appropriate nanostructures can

be superhydrophobic.<sup>13</sup> The pristine surfaces of masks with polymer fibres are smooth at the nanoscale, without superhydrophobic properties. During the last few decades, emerging superhydrophobic coatings with nanostructured surfaces have developed rapidly.<sup>14</sup> Fluorinated polymer,<sup>15</sup> metal nanowires,<sup>16</sup> and graphene<sup>17</sup> have been developed as superhydrophobic coatings. However, to our best knowledge, there is no known report for using these superhydrophobic materials on surgical masks.

Laser induced graphene is a scalable method for producing functional graphene at low cost using commercially available precursors, such as polyimide, SPEEK, bakelite, *etc.*<sup>18</sup> Superhydrophobic states can be obtained by controlling the laser processing environment.<sup>19</sup> By precisely controlling the focus of a near infrared laser beam, the superhydrophobic and superhydrophilic surfaces can be simultaneously generated on opposite sides of the polyimide. The resulting membrane possessed outstanding solar steam generation rates, and could produce 1.3 kg/m<sup>2</sup> fresh water per hour under solar illumination.<sup>20</sup> The superhydrophilic patterns were also patterned on the superhydrophobic surfaces, and could be used to capture sweat droplets on the human body.<sup>21</sup> The additively deposited laser induced graphene *via* continuous wave (CW) laser induced forward transfer (LIFT) showed a superhydrophobic state with highly selective permeability for oil, and can work as an oil recycling device, fully automatic with robots.<sup>22</sup> Due to its photothermal properties, laser induced forward transferred graphene can also be used as anti-bacterial coatings. Owing to its excellent superhydrophobic and photothermal performance, the graphene coating showed 99.9% higher bactericidal performance toward drug-resistant *E. coli* compared to the control sample as glass substrates.<sup>23</sup>

Although the laser scribing graphene is compatible with roll-to-roll production in which modern surgical masks are using. Due to the high processing temperatures of CW-LIFT and the low melting point of the polymer fibers, directly applying this laser induced forward

transfer approach to non-woven masks is challenging.<sup>24</sup> Herein, a dual-mode laser induced forward transfer process has been developed for additively depositing the laser induced graphene onto commercial surgical masks as superhydrophobic and photothermal porous coatings. The self-cleaning capability is enhanced with the use of nanostructure graphene coatings, with the static contact angle of over 140° achieved. With such strong superhydrophobic properties, the water droplets can freely roll without attaching on the mask surface. The surface temperature of the surgical mask can quickly elevate to over 80 °C under solar illumination, which can effectively sterilize the virus. In addition, this mask can also be leveraged for solar desalination after anti-virus use. The resulting solar steam generation rates were higher than 1.13 kg/m<sup>2</sup> per hour under one sun intensity. Due to the micropores within the mask,<sup>25</sup> the mask is also proven to have a better salt rejection performance as compared to polyimide generated membranes, which extends its long-term desalination capabilities.

## **RESULTS and DISCUSSION**

The physical properties of the pristine surgical masks were experimentally studied. The COVID-19 virus is illustrated in Figure 1a and this virus can be spread by touching a polluted surface or by respiration droplets. Since hand hygiene can prevent from direct infection by the polluted surfaces, the masks are primarily used for lowering the infection through respiration droplets generated by sneeze, cough and even talking, to reduce the risk of breathing in these respiration droplets containing viruses into the lungs, as shown in Figure 1b. These commercial surgical masks are mostly fabricated by melt-blown with a non-woven polymer. As a result, the hydrophobic polymer can block most of the respiration droplets from the outside. The microstructures of the pristine masks were characterized using scanning electron microscopy (SEM) as shown in Figure 1c. The melt-blown fibers, with diameters around 20 μm, were randomly distributed. However, it was noted that the surface of these fibers were smooth and lack of superhydrophobic properties, due to the absence of

nanostructures. The surface wetting status of the pristine masks were studied using the static contact angle, as shown in Figure 1d. The measured contact angle of a 5  $\mu$ L water droplet was approximately 110°, which is identified to be hydrophobic. However, the droplets were frequently found to attach to the surface of the mask. The droplets containing viruses would have similar possibility of attaching to the surfaces of commercial surgical masks. So there is plenty of room for improving the protection performance of pristine surgical masks with superhydrophobic surfaces.

Superhydrophobic surfaces for surgical masks can be realized in the present study by using the laser induced forward transfer of laser synthesized graphene. The non-woven polymer within the pristine surgical masks are made of thermoplastics such as polypropylene.<sup>26</sup> Due to their low melting points, the direct laser transferred graphene using the previously reported methods would result in damaged structures on the masks.<sup>23</sup> The first-generation laser induced graphene *via* directly scribing on polyimide cannot be used to create graphene on the mask, due to the remained polyimide after CO<sub>2</sub> laser scribing as shown in Figure 2a.<sup>27</sup> Although the second-generation laser scribe graphene using 1064 nm can create the Janus wetting status on the opposite sides of the polyimide, it is impossible to transfer the synthesized graphene to the mask, as shown in Figure 2b.<sup>20</sup> The third-generation CW LIFT graphene can be deposited additively onto other substrates, as shown in Figure 2c.<sup>24</sup> However, the high temperature on the targeted acceptors had significant influence on their final morphology and damage the surgical masks. After the CW-LIFT was applied on the masks, the surface layers of the masks tend to melt due to the high temperatures, as shown in Figure S1. The melting temperature of the non-woven mask was measured to be lower than 130 °C, as shown in Figure S2 and S3. To overcome this challenge, an additional pulse laser induced forward transfer (pulse-LIFT) following the CW LIFT is adopted,<sup>28,29</sup> as shown in Figure 2d. The polyimide film is firstly simultaneously synthesized and laser forward

transferred from the bottom to the upper polyimide film using a CW mode laser. Hence, the transferred graphene is moved to the second laser using pulse mode, which further transfers the synthesized graphene onto the mask surfaces. With a pulse width of 10 ns, the momentum of the photons is utilized as kinetic energy to transfer the graphene.<sup>30</sup> At sufficiently low temperature, the graphene can be coated onto the surgical mask without damaging its surfaces. This fourth-generation laser deposition method is also compatible with roll-to-roll system, which can be easily integrated within the existing automatic mask manufacturing production lines, as shown in Figure 2e.

The microstructural and physical properties of the laser transferred graphene are systematically characterized. An optical image of the graphene coated masks is shown in Figure 3a. The black colour on the pristine white mask indicates the transferred carbon on its surface. The microstructures of the coated materials were examined using a scanning electron microscope, as shown in Figure 3b. Differing from the smooth surfaces of the microfibers, as compared in Figure 1c, the nanostructured flakes were observed all over the fiber surfaces, with sizes randomly distributed from 100 nm to a few micrometres. To identify the chemical composition of these nanoflakes, their phonon vibration modes were studied using Raman spectra analysis, as shown in Figure 3c. The dominant D, G and 2D peaks at 1330, 1570 and 2665  $\text{cm}^{-1}$ , and weak D+G peaks at 2898  $\text{cm}^{-1}$  clearly indicate the presence of graphene. According to the position of the 2D peak and the relative intensity ratio of the 2D peak over the D peak, the coatings can be identified as few-layer graphene.<sup>31</sup> To study the non-wetting enhancement of the mask, the static contact angle of the graphene coated mask was measured to be 141°, as shown in Figure 3d. It was also found that the water droplets had great difficulty to stay on the surface due to the strong superhydrophobic effect, like that of a lotus leaf.<sup>32</sup> As a result, the dynamic wetting properties were also studied, as shown in the supplementary video M1. It was observed that the water droplet moved freely on the surfaces

of the graphene coated mask, without leaving any observed droplets behind. So the outstanding superhydrophobic properties of graphene coating can significantly improve the self-cleaning performance for the respiratory droplets, as shown in Figure 3e.

To sterilize the potentially remaining viruses on the surface of the graphene coated mask, their photothermal performances were experimentally studied. The optical absorption of the surgical masks is depicted in Figure 4a. The pristine masks had low absorption toward solar spectra, especially in the visible and near infrared regions. In contrast, the graphene coating masks showed over 95% absorption across the whole solar spectrum from 300 nm to 2500 nm. The COVID-19 use the spike virus for infection through the Angiotensin-converting enzyme 2 (ACE2).<sup>33</sup> Since the spike protein on COVID-19 virus is sensitive to temperature, which enables the photothermal graphene coated mask a promising feature for self-sterilization.<sup>34</sup> The photothermal properties were studied by measuring the surface temperatures of the coated and control samples under 1 sun intensity using a solar simulator. As shown in Figure 4b, the temperature of the pristine mask increased and stayed lower than 45 °C after 5 min of solar illumination. In comparison, the surface temperatures of the graphene coated masks were quickly elevated over 70 °C after 40 seconds of solar illumination, and they stayed over 80 °C after 100 seconds of solar illumination, which is consistent with the photothermal performance of literature.<sup>35</sup> According to the virus sterilization information, a temperature over 70 °C is sufficiently high for inactivating most types of viruses.<sup>36, 37</sup> The overall temperature distribution of the graphene coated mask and the pristine mask were also characterized using an infrared camera under 5 minutes solar illumination, with uniform heating across the coated regions and the pristine mask surface, as shown in Figure 4c and 4d, respectively. However, the surface temperature of the pristine surgical mask did not exceed 50 °C even after 5 min solar illumination as shown in the Figure S7, so it lacked the photothermal sterilization capabilities. As a result, this graphene coated

mask significantly contributes to self-sterilize for those potentially remaining viruses *via* solar illumination.<sup>23</sup>

After the virus is erased from the earth hopefully in the near future, these graphene coated masks also have high potential to be recycled for other applications. Due to the outstanding photothermal performance and the porous structures, the masks can be directly used as solar steam generators, as illustrated in Figure 5a. After 30 min of solar illumination, the temperature of the graphene coated mask was stabilized at 36 °C, while the temperature of the bulk water was increased from 21 °C to 24 °C, as shown in Figure S9. So it can be indicated that the interfacial solar desalination was mainly located at the graphene coated mask, without significantly heating up the bulk water. The graphene coated masks achieved a 1.13 kg/m<sup>2</sup> per hour solar steam generation rate as shown in Figure 5b, which is sufficiently high for small scale desalination using solar energy. Although the evaporation rates were lower than that reported in state-of-art research, it was still higher than the pristine mask with the solar evaporation rate at only 0.3 kg/m<sup>2</sup>h, as shown in Figure S8. The low evaporation rates are due to the lack of hydrophilic absorption layers on the masks and the water transportation medium within the mask tri-layer structures. The evaporating performances can be further enhanced in future work by incorporating these functional materials, such as PVA.<sup>38, 39</sup> Meanwhile, the graphene coated masks showed outstanding long-term stability and salt-rejection functions for desalination. For evaporating 10 wt% salt water, the graphene coated masks showed significantly better performance toward salt rejection, as shown in Figure 5c, compared to reported solar steam generators using laser scribed polyimide.<sup>20</sup> The micropores within the microscale fiber can contribute to better salt dissolving channels. There was no noticeable salt accumulation on the surfaces of the graphene coated masks, with stable steam generation rate over 1 kg/m<sup>2</sup>h for 100 hours continuous evaporating. This demonstrates that it is technically feasible for the long-term solar desalination.

This graphene coated mask fabricated by dual-mode laser scribing showed outstanding superhydrophobic and photothermal performance, with great reusable and recyclable potentials. The dual mode LIFT overcomes the challenges of the temperature sensitivity of the masks, which is significantly advanced compared to the reported laser induced graphene. The roll-to-roll compatible laser manufacturing process can also be integrated to current roll-to-roll surgical mask production lines. The superhydrophobic surfaces provide better protection toward outside viruses containing droplets through the self-cleaning coating. Even though there might be some viruses attached to the surfaces of the mask, they can be quickly sterilized by the high surface temperature over 80 °C under sunlight. The reusability of this graphene mask should satisfy 3 conditions: the maintenance of the mask structure, superhydrophobic and photothermal properties. The SEM images (Figure S4) of masks after 24, 48 and 72 hours of sun illumination indicated that the graphene coating did not suffer any noticeable influence after long term solar illumination as sterilization. The results of the contact angle test (Figure S5) and the surface temperature measurement (Figure S6) indicated the feasibility of applications from the recycled masks, with no declining performances in the superhydrophobic and photothermal features. Therefore, the recycled mask can also be used in solar steam generation, with usable solar steam generation rates and outstanding salt-rejection performance. The price for polyimide films as raw materials is also low, estimated to 0.05 USD for fabricating each graphene mask, which is practical for mass production. So these reusable and recyclable masks can provide economic, environmentally friendly solutions and better protection for fighting the raging COVID-19 virus pandemic. However, there are some limitations in the current research using the reported laser scribed methods. Although the graphene showed a relatively high optical absorption, its adsorption is not as high as 100%. The addition of plasmonic nanoparticles as composite coatings can help to improve the solar energy absorption.<sup>40</sup> The hydrophobic nature of the non-woven fibers

hinders water absorption from bulk seawater and transportation within the device, resulting in a low evaporation rate. This can be improved by the addition of superhydrophilic structures and sol-gel polymers for enhancing the water absorption and transportation.<sup>41, 42</sup> Further enhancement of the thermal transfer within the masks can also help improve the desalination rates.<sup>43, 44</sup> There are also some defects observed at the edge of the folded region, and this can be overcome in real production conditions by having the laser deposition processes prior the folding processes of the non-woven fibers. At the same time, the virus filtration properties of these graphene coated masks are highly dependent on the pristine surgical masks. Although we have already proved the photothermal and superhydrophobic anti-bacterial performances of CW-LIFT graphene against *E.coli*,<sup>23</sup> the actual virus protection performance of these masks coated with pulse-LIFT graphene still needs to be confirmed. Meanwhile, some more advanced methods with superhydrophobic and photothermal properties are foreseen to appear for integrating into surgical masks. Significant efforts will be devoted to overcoming these challenges for fabricating superhydrophobic coating masks, such as using hydrothermal synthesis methods for temperature sensitive masks, the growth of nanowires on electrical insulating masks, and spray coating on hydrophobic pristine masks. It is believed that there will be more advanced masks with enhanced performance in the near future to defeat the virus outbreak.

## **CONCLUSIONS**

On the whole, a dual-mode laser fabrication method for additively depositing few-layer graphene on temperature sensitive surgical masks is presented. The superhydrophobic surfaces provide better protection toward incoming respiration droplets. The high surface temperatures of the masks under solar illumination can sterilize the surface viruses. Recycled graphene coated masks can also work as solar steam generation devices with salt-rejection performance for long-term usage. It is foreseen that better performance will be achieved from

the future research which can be inspired by this work, with masks fabricated by more advanced materials.

## **METHODS**

### **FABRICATION of the FUNCTIONAL MASK**

The surgical masks and polyimide films were used directly after purchase without any treatment. A DMG Lasertec 40 laser machining system was used for both the CW and pulse mode scribing, with 1064 nm wavelength, 3 W power, 400 mm/s scan speed and 20  $\mu\text{m}$  spot size. The laser beam was focused on the donor polyimide film. During the scanning of laser beam using the CW mode, the graphene flakes can be synthesized and forward deposited to the acceptor polyimide, with a 1 mm spacer between the donor and acceptor. Then, the transferred coated graphene in the upper polyimide (Figure 2d) was further deposited onto the surgical mask at low temperature performed by pulsed-LIFT with a 1 mm spacer, using 1064 nm wavelength with 0.7 W power, 10 ns pulse width and 400 mm/s speed.

### **CHARACTERIZATION of the MASK**

A Newport 91160 solar simulator (Air Mass 1.5 sunlight) was used for the evaporation tests with intensity calibrated to 1,000  $\text{W}/\text{m}^2$ . The microstructures of the masks were characterized by a Tescan VEGA3 SEM. The static contact angle was measured by a Sindatek 100SB optical contact angle meter using the sessile drop method. The Raman spectra was characterized with a LabRAM HR 800 Raman Spectrometer using a 532 nm laser source. The thermal conductivity was measured by an Anter Flashline 2000 Thermal Conductivity Analyzer. The surface temperatures of the samples were measured by a Fluke Ti200 infrared camera. The optical absorption spectrum was measured by a Hitachi UH4150 spectrophotometer equipped with integrating sphere.

## **SUPPORTING INFORMATION**

The Supporting Information is available free of charge on the ACS Publication website at  
[Online link]

Experimental additional characterization data: Optical image of the mask after 3<sup>rd</sup> generation CW-LIFT graphene; the optical image of the melted mask; the experimental setup for measuring the melting point of the pristine mask; SEM images for masks under aging test; water contact angles of masks; infrared images of the masks after 72 h solar sterilization; the measured temperature of graphene coated mask and the pristine masks against time; desalination efficient of original mask; solar steam generator (PDF)

Video M1: Superhydrophobic property of the graphene coated mask (avi)

## ACKNOWLEDGEMENTS

The work described in this paper was mainly supported by the funding support to the State Key Laboratories in Hong Kong from the Innovation and Technology Commission (ITC) of the Government of the Hong Kong Special Administrative Region (HKSAR), China. The authors would also like to express their sincerely thanks to the financial support from the Research Office (Project code: BBX7 and BBX9) of Hong Kong Polytechnic University.

## REFERENCES

1. Wang, H.; Wang, Z.; Dong, Y.; Chang, R.; Xu, C.; Yu, X.; Zhang, S.; Tsamlag, L.; Shang, M.; Huang, J.; Wang, Y.; Xu, G.; Shen, T.; Zhang, X.; Cai, Y., Phase-Adjusted Estimation of the Number of Coronavirus Disease 2019 Cases in Wuhan, China. *Cell Discovery* **2020**, *6*, 10.
2. Leung, C. C.; Lam, T. H.; Cheng, K. K., Mass Masking in the COVID-19 Epidemic: People Need Guidance. *The Lancet* **2020**, 395, 945.
3. Addi, R. A.; Benksim, A.; Cherkaoui, M., Easybreath Decathlon Mask: An Efficient Personal Protective Equipment (PPE) against COVID-19 in Africa. *Journal of Clinical and Experimental Investigations* **2020**, *11*, em00738.
4. Makison Booth, C.; Clayton, M.; Crook, B.; Gawn, J. M., Effectiveness of Surgical Masks against Influenza Bioaerosols. *J. Hosp. Infect.* **2013**, *84*, 22-26.
5. MacIntyre, C. R.; Chughtai, A. A., Facemasks for the Prevention of Infection in Healthcare and Community Settings. *BMJ : British Medical Journal* **2015**, *350*, h694.

6. Leung, N. H. L.; Chu, D. K. W.; Shiu, E. Y. C.; Chan, K.-H.; McDevitt, J. J.; Hau, B. J. P.; Yen, H.-L.; Li, Y.; Ip, D. K. M.; Peiris, J. S. M.; Seto, W.-H.; Leung, G. M.; Milton, D. K.; Cowling, B. J., Respiratory Virus Shedding in Exhaled Breath and Efficacy of Face Masks. *Nat. Med.* **2020**, DOI: 10.1038/s41591-020-0843-2.
7. Booth, C. M.; Clayton, M.; Crook, B.; Gawn, J.; Effectiveness of Surgical Masks against Influenza Bioaerosols. *J. Hosp. Infect.* **2013**, *84*, 22-26.
8. Shen, H.; Leonas, K., Study of Repellent Finish of Filtration Ability of Surgical Face Masks. *International Nonwovens Journal* **2005**, *os-14*, 1558925005os-14.
9. Majchrzycka, K.; Okrasa, M.; Szulc, J.; Jachowicz, A.; Gutarowska, B., Survival of Microorganisms on Nonwovens Used for the Construction of Filtering Facepiece Respirators. *Int. J. Environ. Res. Public Health* **2019**, *16*, 1154.
10. Wu, T.; Li, H.; Xue, J.; Mo, X.; Xia, Y., Photothermal Welding, Melting, and Patterned Expansion of Nonwoven Mats of Polymer Nanofibers for Biomedical and Printing Applications. *Angew. Chem.* **2019**, *131*, 16568-16573.
11. Alam, Q.; Schollbach, K.; Rijnders, M.; van Hoek, C.; van der Laan, S.; Brouwers, H., The Immobilization of Potentially Toxic Elements Due to Incineration and Weathering of Bottom Ash Fines. *J. Hazard. Mater.* **2019**, *379*, 120798.
12. Tian, X.; Verho, T.; Ras, R. H., Moving Superhydrophobic Surfaces toward Real-World Applications. *Science* **2016**, *352*, 142-143.
13. Lafuma, A.; Quéré, D., Superhydrophobic States. *Nat. Mater.* **2003**, *2*, 457-460.
14. Liu, M.; Wang, S.; Jiang, L., Nature-Inspired Superwettability Systems. *Nat. Rev. Mater.* **2017**, *2*, 17036.
15. Wang, H.; Xue, Y.; Ding, J.; Feng, L.; Wang, X.; Lin, T., Durable, Self-Healing Superhydrophobic and Superoleophobic Surfaces from Fluorinated-Decyl Polyhedral Oligomeric Silsesquioxane and Hydrolyzed Fluorinated Alkyl Silane. *Angew. Chem.* **2011**, *50*, 11433-11436.
16. Lo, C. W.; Wang, C. C.; Lu, M. C., Spatial Control of Heterogeneous Nucleation on the Superhydrophobic Nanowire Array. *Adv. Funct. Mater.* **2014**, *24*, 1211-1217.
17. Lee, J.-S.; Yoon, J.-C.; Jang, J.-H., A Route towards Superhydrophobic Graphene Surfaces: Surface-Treated Reduced Graphene Oxide Spheres. *J. Mater. Chem. A* **2013**, *1*, 7312-7315.
18. Li, G., Direct Laser Writing of Graphene Electrodes. *J. Appl. Phys.* **2020**, *127*, 010901.
19. Li, Y.; Luong, D. X.; Zhang, J.; Tarkunde, Y. R.; Kittrell, C.; Sargunraj, F.; Ji, Y.; Arnusch, C. J.; Tour, J. M., Laser-Induced Graphene in Controlled Atmospheres: From Superhydrophilic to Superhydrophobic Surfaces. *Adv. Mater.* **2017**, *29*, 1700496.
20. Li, G.; Law, W.-C.; Chan, K. C., Floating, Highly Efficient, and Scalable Graphene Membranes for Seawater Desalination Using Solar Energy. *Green Chem.* **2018**, *20*, 3689-3695.
21. Li, G.; Mo, X.; Law, W.-C.; Chan, K. C., Wearable Fluid Capture Devices for Electrochemical Sensing of Sweat. *ACS Appl. Mater. Interfaces* **2019**, *11*, 238-243.
22. Li, G.; Mo, X.; Wang, Y.; Chan, C.-Y.; Chan, K. C., All 3D-Printed Superhydrophobic/Oleophilic Membrane for Robotic Oil Recycling. *Adv. Mater. Interfaces* **2019**, *6*, 1900874.
23. Jiang, N.; Wang, Y.; Chan, K. C.; Chan, C.-Y.; Sun, H.; Li, G., Additive Manufactured Graphene Coating with Synergistic Photothermal and Superhydrophobic Effects for Bactericidal Applications. *Global Challenges* **2020**, *4*, 1900054.
24. Li, G.; Mo, X.; Law, W.-C.; Chan, K. C., 3D Printed Graphene/Nickel Electrodes for High Areal Capacitance Electrochemical Storage. *J. Mater. Chem. A* **2019**, *7*, 4055-4062.

25. Ni, G.; Zandavi, S. H.; Javid, S. M.; Boriskina, S. V.; Cooper, T. A.; Chen, G., A Salt-Rejecting Floating Solar Still for Low-Cost Desalination. *Energy Environ. Sci.* **2018**, *11*, 1510-1519.
26. Lee, Y.; Wadsworth, L. C., Structure and Filtration Properties of Melt Blown Polypropylene Webs. *Polym. Eng. Sci.* **1990**, *30*, 1413-1419.
27. Li, G.; Meng, Z.; Qian, J.; Ho, C.-L.; Lau, S. P.; Wong, W.-Y.; Yan, F., Inkjet Printed Pseudocapacitive Electrodes on Laser-Induced Graphene for Electrochemical Energy Storage. *Materials Today Energy* **2019**, *12*, 155-160.
28. Tseng, M. L.; Chen, B. H.; Chu, C. H.; Chang, C. M.; Lin, W. C.; Chu, N.-N.; Mansuripur, M.; Liu, A. Q.; Tsai, D. P., Fabrication of Phase-Change Chalcogenide Ge<sub>2</sub>Sb<sub>2</sub>Te<sub>5</sub> Patterns by Laser-Induced Forward Transfer. *Opt. Express* **2011**, *19*, 16975-16984.
29. Tseng, M. L.; Wu, P. C.; Sun, S.; Chang, C. M.; Chen, W. T.; Chu, C. H.; Chen, P. L.; Zhou, L.; Huang, D. W.; Yen, T. J.; Tsai, D. P., Fabrication of Multilayer Metamaterials by Femtosecond Laser-Induced Forward-Transfer Technique. *Laser & Photon. Rev.* **2012**, *6*, 702-707.
30. Visser, C. W.; Pohl, R.; Sun, C.; Römer, G.-W.; Huis in 't Veld, B.; Lohse, D., Toward 3D Printing of Pure Metals by Laser-Induced Forward Transfer. *Adv. Mater.* **2015**, *27*, 4087-4092.
31. Graf, D.; Molitor, F.; Ensslin, K.; Stampfer, C.; Jungen, A.; Hierold, C.; Wirtz, L., Spatially Resolved Raman Spectroscopy of Single- and Few-Layer Graphene. *Nano Lett.* **2007**, *7*, 238-242.
32. Wang, P.; Zhao, T.; Bian, R.; Wang, G.; Liu, H., Robust Superhydrophobic Carbon Nanotube Film with Lotus Leaf Mimetic Multiscale Hierarchical Structures. *ACS Nano* **2017**, *11*, 12385-12391.
33. Zheng, Y.-Y.; Ma, Y.-T.; Zhang, J.-Y.; Xie, X., Covid-19 and the Cardiovascular System. *Nat. Rev. Cardiol.* **2020** *17*, 259–260.
34. Henwood, A. F., Coronavirus Disinfection in Histopathology. *J. Histotechnol.* **2020**, DOI: 10.1080/01478885.2020.1734718.
35. Lin, K.-T.; Lin, H.; Yang, T.; Jia, B., Structured Graphene Metamaterial Selective Absorbers for High Efficiency and Omnidirectional Solar Thermal Energy Conversion. *Nat. Commun.* **2020**, *11*, 1389.
36. Maheshwari, G.; Jannat, R.; McCormick, L.; Hsu, D., Thermal Inactivation of Adenovirus Type 5. *J. Virol. Methods* **2004**, *118*, 141-146.
37. Mocé-Llivina, L.; Muniesa, M.; Pimenta-Vale, H.; Lucena, F.; Jofre, J., Survival of Bacterial Indicator Species and Bacteriophages after Thermal Treatment of Sludge and Sewage. *Appl. Environ. Microbiol.* **2003**, *69*, 1452-1456.
38. Zhu, L. L.; Ding, T. P.; Gao, M. M.; Peh, C. K. N.; Ho, G. W., Shape Conformal and Thermal Insulative Organic Solar Absorber Sponge for Photothermal Water Evaporation and Thermoelectric Power Generation. *Adv. Energy Mater.* **2019**, *9*.
39. Xu, W. Z.; Xing, Y.; Liu, J.; Wu, H. P.; Cuo, Y.; Li, D. W.; Guo, D. Y.; Li, C. R.; Liu, A. P.; Bai, H., Efficient Water Transport and Solar Steam Generation via Radially, Hierarchically Structured Aerogels. *ACS Nano* **2019**, *13*, 7930-7938.
40. Zhou, L.; Tan, Y. L.; Wang, J. Y.; Xu, W. C.; Yuan, Y.; Cai, W. S.; Zhu, S. N.; Zhu, J., 3D Self-Assembly of Aluminium Nanoparticles for Plasmon-Enhanced Solar Desalination. *Nat. Photonics* **2016**, *10*, 393-399.
41. Nandakumar, D. K.; Zhang, Y. X.; Ravi, S. K.; Guo, N.; Zhang, C.; Tan, S. C., Solar Energy Triggered Clean Water Harvesting from Humid Air Existing above Sea Surface Enabled by a Hydrogel with Ultrahigh Hygroscopicity. *Adv. Mater.* **2019**, *31*, 1806730.

42. Mu, P.; Zhang, Z.; Bai, W.; He, J. X.; Sun, H. X.; Zhu, Z. Q.; Liang, W. D.; Li, A., Superwetting Monolithic Hollow-Carbon-Nanotubes Aerogels with Hierarchically Nanoporous Structure for Efficient Solar Steam Generation. *Adv. Energy Mater.* **2019**, *9*, 1802158.
43. Alabastri, A.; Dongare, P. D.; Neumann, O.; Metz, J.; Adebiyi, I.; Nordlander, P.; Halas, N. J., Resonant Energy Transfer Enhances Solar Thermal Desalination. *Energy Environ. Sci.* **2020**, *13*, 968-976.
44. Dongare, P. D.; Alabastri, A.; Neumann, O.; Nordlander, P.; Halas, N. J., Solar Thermal Desalination as a Nonlinear Optical Process. *Proceedings of the National Academy of Sciences* **2019**, *116*, 13182-13187.

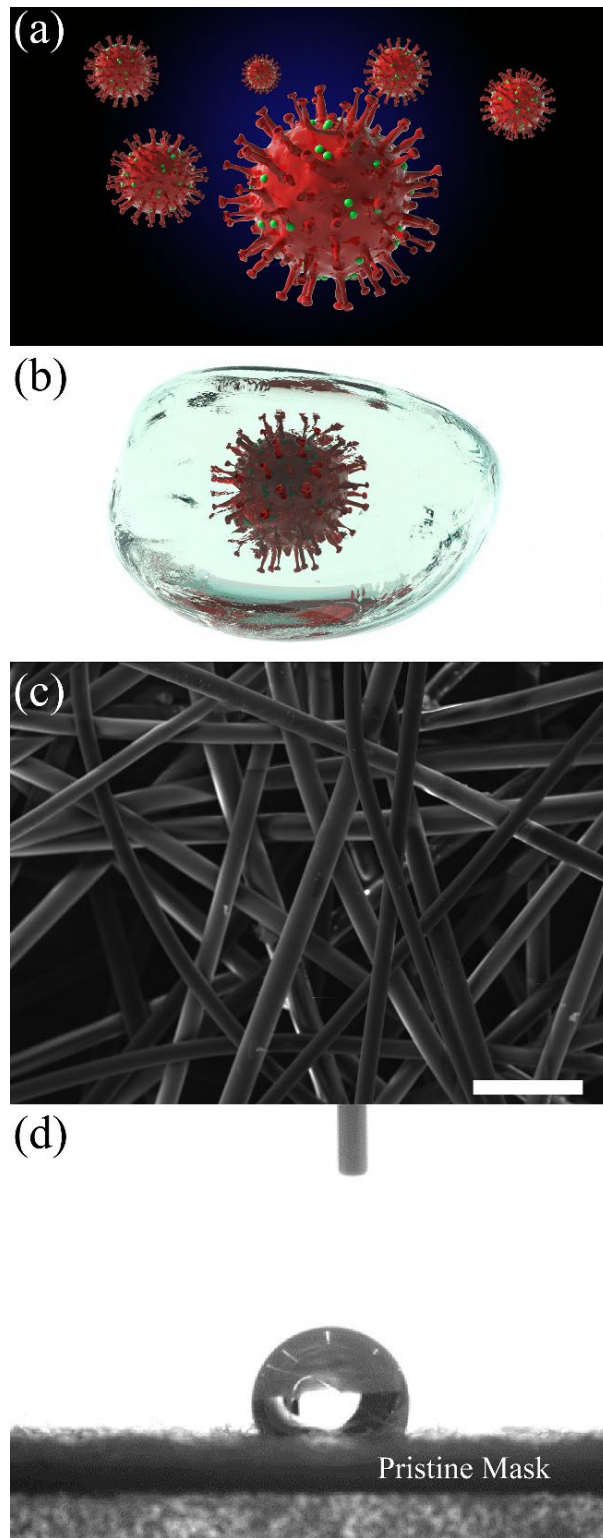


Figure 1. (a) Illustration schematics of the COVID-19 viruses. (b) Illustration of respiration droplet containing a COVID-19 virus. (c) SEM image of the non-woven fibers from the pristine surgical mask, the scale bar is 100  $\mu\text{m}$ . (d) The water contact angle measurement of the pristine surgical mask.

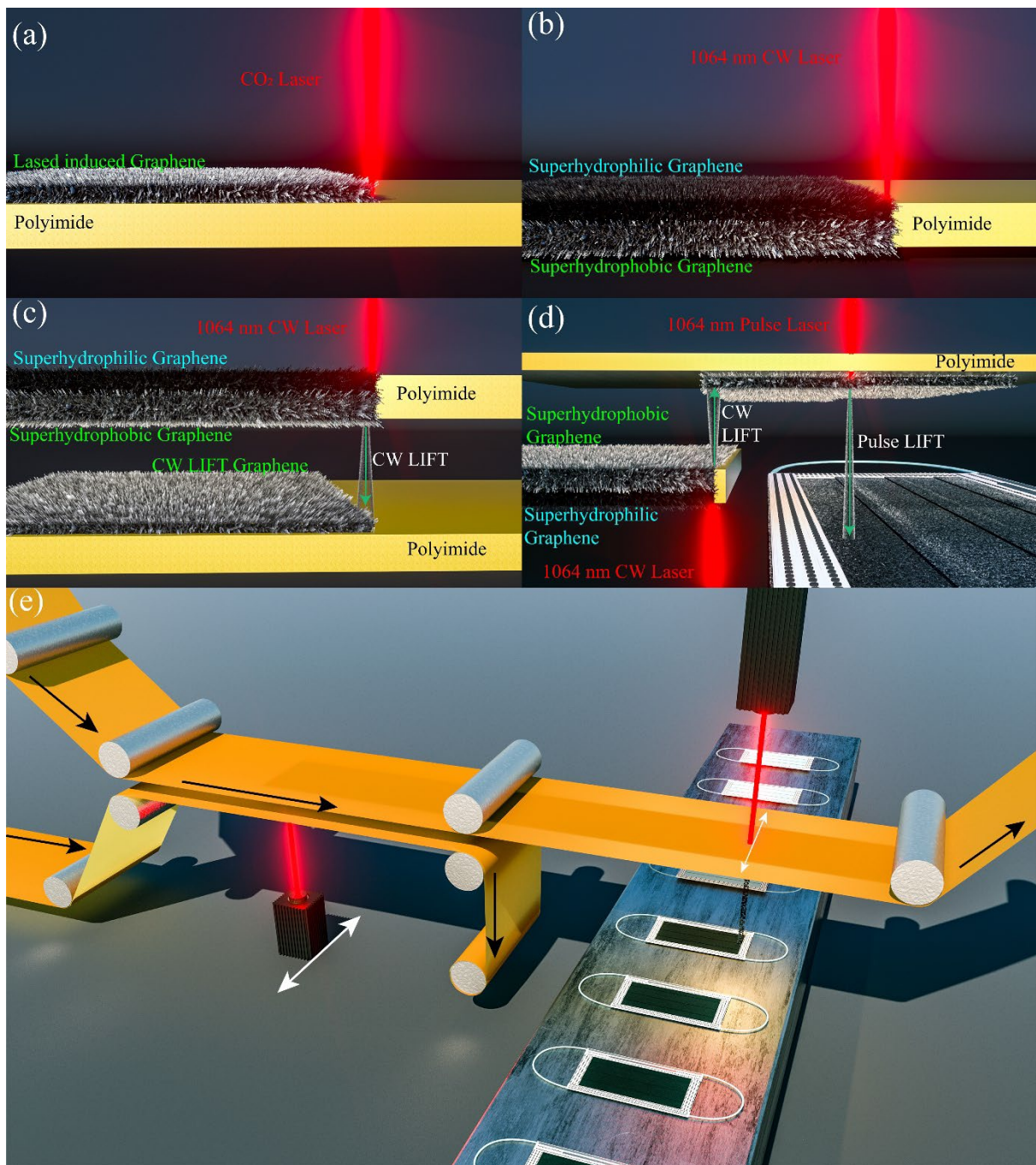


Figure 2. Comparison of different laser induced graphene methods. (a) 1<sup>st</sup> generation direct laser induced graphene on polyimide surface using CO<sub>2</sub> laser.<sup>27</sup> (b) 2<sup>nd</sup> generation Janus superhydrophobic/superhydrophilic by 1064 nm laser scribing on polyimide.<sup>20</sup> (c) 3<sup>rd</sup> generation CW-LIFT of graphene from polyimide to acceptor polyimide.<sup>24</sup> (d) 4<sup>th</sup> generation dual-mode LIFT, with CW-LIFT transfer graphene onto second polyimide, and then pulse-LIFT transfer graphene onto temperature sensitive mask. (e) Illustration of the compatibility

of the dual-mode LIFT for roll-to-roll production of graphene coated mask. The roll movement direction is shown as the black arrow and the laser movement direction is indicated by the white arrows.

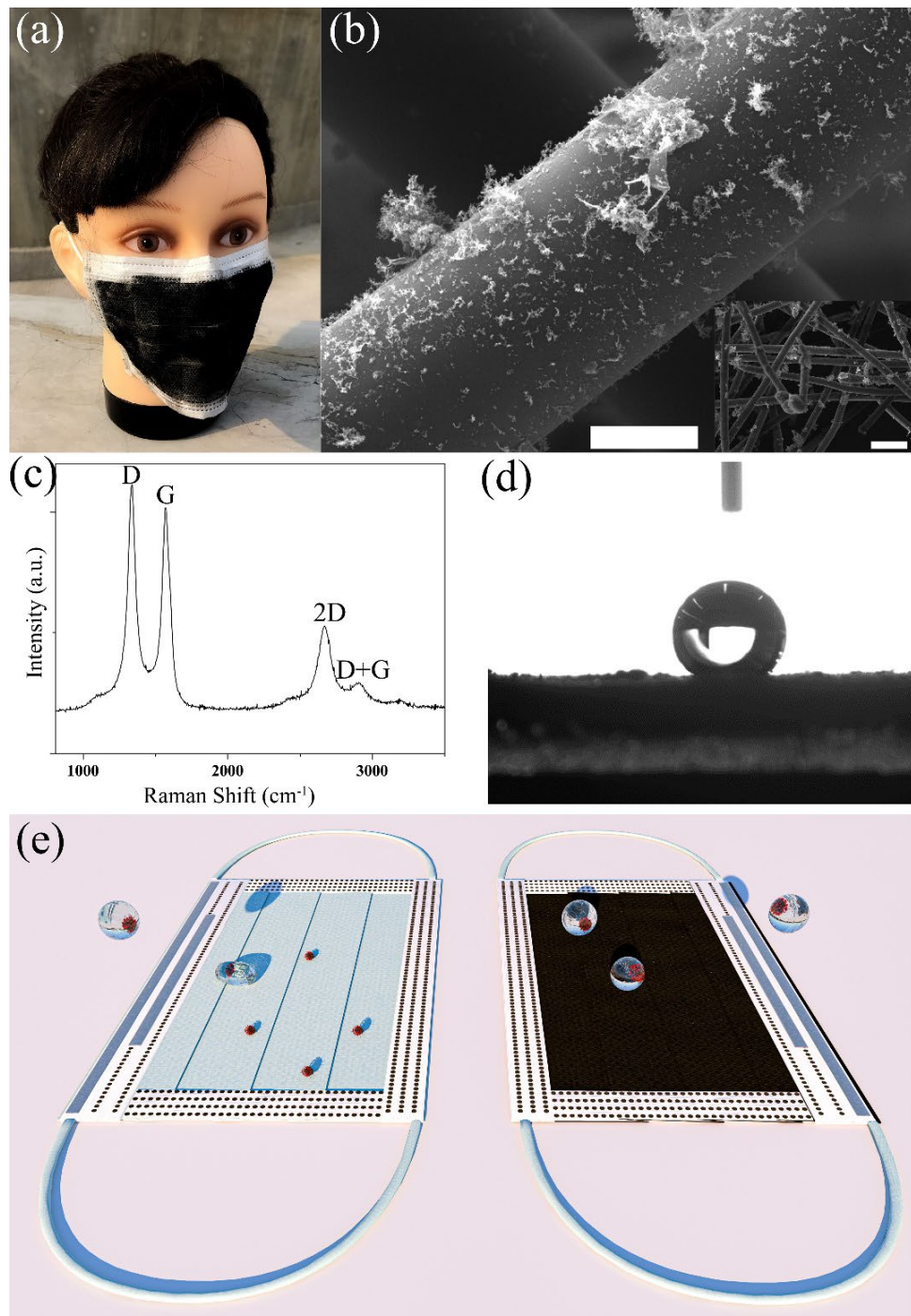


Figure 3. (a) Optical image of the laser fabricated graphene mask. (b) SEM of the graphene coated non-woven fiber within the surgical mask, scale bar 10 μm. The inset is the zoom-out

image, with the scale bar at 100  $\mu\text{m}$ . (c) Raman spectra of the graphene coated mask. (d) Water contact angle on the graphene coated mask. (e) Illustration of the self-cleaning properties of the black graphene coated mask (right), compared to the pristine blue mask(left).

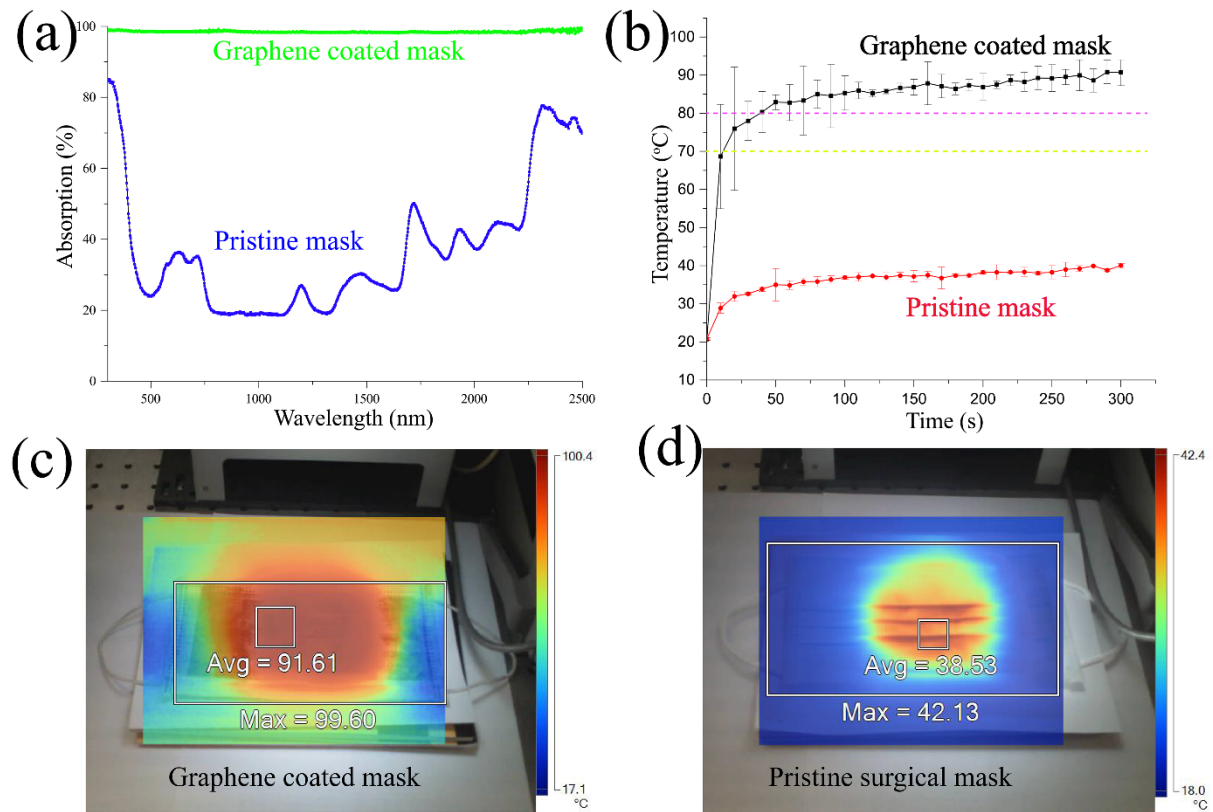


Figure 4. Photothermal performance of the masks. (a) Optical absorption of pristine and graphene coated masks. (b) Surfaces temperature measured by infrared camera against time, for graphene coated masks and pristine masks. The infrared camera images of (c) graphene coated mask (d) pristine surgical mask after 5 minutes solar illumination.

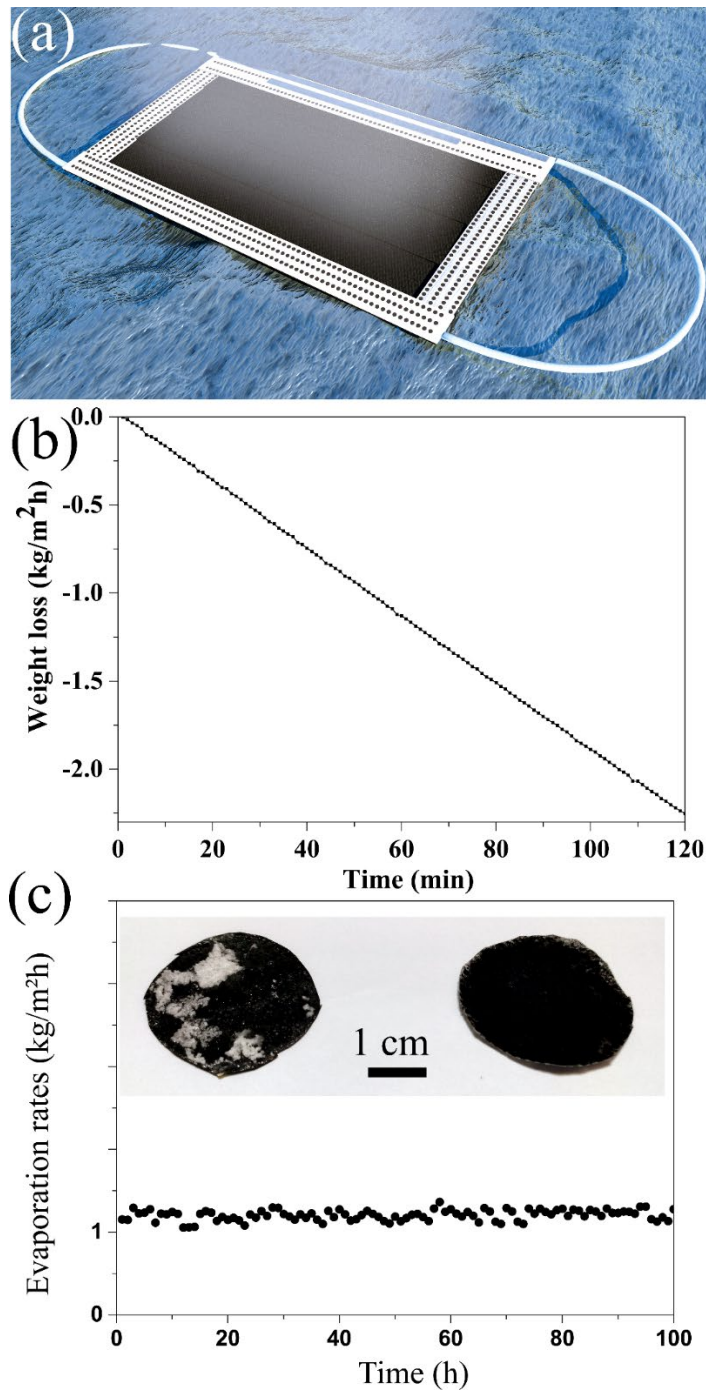


Figure 5. Solar steam generation performance of the graphene coated masks. (a) Illustration of the floating graphene coated mask for solar desalination. (b) The weight loss of 10%wt saltwater with the graphene coated mask under 1 sun intensity. (c) Upper: Salt rejection performance capture photos of the polyimide after laser scribing after 4 hours desalination(left), graphene coated mask after 100 hours desalination(right); Bottom: The evaporation rates of the graphene coated mask under 1 sun intensity.

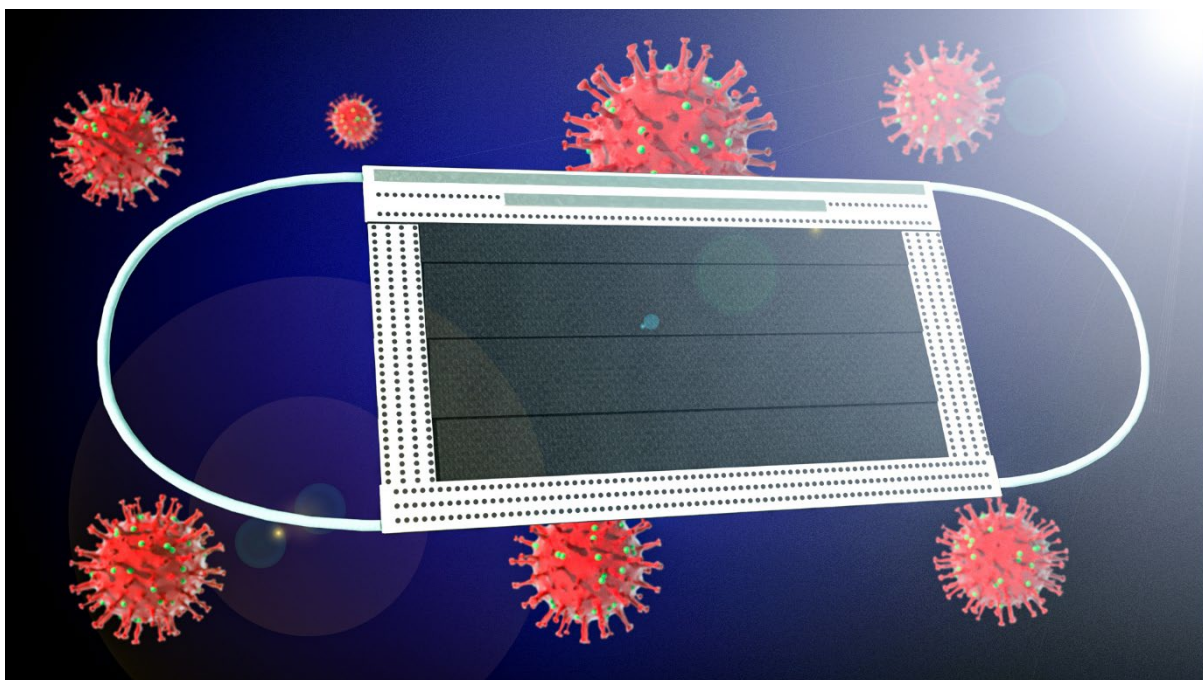


Table of content

The graphene masks with excellent photothermal and superhydrophobic features provide better protection against COVID-19.